UCLA
UCLA Previously Published Works

Title
Formation of a Ti–Cu(111) single atom alloy: Structure and CO binding

Permalink
https://escholarship.org/uc/item/307940dx

Journal
The Journal of Chemical Physics, 154(23)

ISSN
0021-9606

Authors
Shi, Junjie
Owen, Cameron J
Ngan, Hio Tong
et al.

Publication Date
2021-06-21

DOI
10.1063/5.0050800

Supplemental Material
https://escholarship.org/uc/item/307940dx#supplemental

Peer reviewed

eScholarship.org Powered by the California Digital Library
University of California

Formation of a Ti-Cu(111) Single Atom Alloy: Structure and CO Binding

Junjie Shi[1], Cameron J. Owen[2], Hio Tong Ngan[3], Siyu Qin[1], Vikram Mehar[1], Philippe Sautet[3,4*] and Jason F. Weaver[1]*

[1]Department of Chemical Engineering, University of Florida, Gainesville, FL 32611, USA
[2] Department of Chemistry and Chemical Biology, Harvard University, Cambridge, MA 02138, USA
[3]Department of Chemical and Biomolecular Engineering, University of California, Los Angeles, Los Angeles, California 90095, USA
[4]Department of Chemistry and Biochemistry, University of California, Los Angeles, Los Angeles, California 90095, USA

Corresponding author emails:
*sautet@ucla.edu
*weaver@che.ufl.edu

Abstract

A single atom Ti-Cu(111) surface alloy can be generated by depositing small amounts of Ti onto Cu(111) at slightly elevated surface temperatures (~500-600 K). Scanning tunneling microscopy shows that small Ti-rich islands covered by a Cu single layer form preferentially on ascending step edges of Cu(111) during Ti deposition below about 400 K, but that a Ti-Cu(111) alloy replaces these small islands during deposition between 500 and 600 K, producing an alloy in the brims of the steps. Larger partially Cu-covered Ti containing islands also form on the Cu(111) terraces at temperatures between 300 and 700 K. After surface exposure to CO at low temperature, reflection absorption infrared spectroscopy (RAIRS) reveals distinct C-O stretch bands at 2102 cm^{-1} and 2050 cm^{-1} attributed to CO adsorbed on Cu-covered Ti containing domains vs. sites in the Ti-Cu(111) surface alloy, respectively. Calculations using density functional theory (DFT) suggest that the lower frequency C-O stretch band originates specifically from CO adsorbed on isolated Ti atoms in the Ti-Cu(111) surface alloy, and predicts a higher C-O stretch frequency for CO adsorbed on Cu above subsurface Ti ensembles. DFT further predicts that CO preferentially adsorbs in flat-lying configurations on contiguous Ti surface structures with more than one Ti atom and thus that CO adsorbed on such structures should not be observed with RAIRS. The ability to generate a single atom Ti-Cu(111) alloy will provide future opportunities to investigate the surface chemistry promoted by a representative early transition metal dopant in a Cu(111) host surface.

Introduction

Single atom alloys (SAA) have emerged as a special class of catalytic materials due to their unique surface electronic properties and ability to promote selective chemical transformations.[1-5] In catalysis, SAAs are generally formed by dispersing low concentrations of a transition metal into the surface layer of a coinage metal (Cu, Ag, Au) so that individual transition metal atoms are isolated from another, surrounded only by atoms of the host metal. The transition metal atoms serve as reactive centers and their isolation in the host surface can promote selective chemistry in part by preventing multiple-step routes to undesirable products. Most prior studies have focused on SAAs of coinage metals doped with small amounts of a late transition metal (Pt, Pd, Rh, Ni, Ru) and indeed these SAAs have been shown to selectively promote a diverse range of chemistries, including hydrogenation and dehydrogenation reactions, C-C and C-O coupling, NO reduction and CO oxidation.[2,6-12]

Compared with late transition metal SAAs, dilute alloys of coinage metals doped with early transition metals have received limited attention but are likely to exhibit distinct surface chemical properties. For instance, the high oxophilicity of early transition metals could lead to preferential activation and functionalization of O-containing functional groups of organic compounds, enabling chemistries such as the selective hydrogenation of unsaturated aldehydes to alkenols.[13] Recent calculations using density functional theory (DFT) also predict that several early transition metal SAAs are capable of activating CH_4 at low temperature.[4] This prediction suggests possibilities for selectively converting alkanes to value-added products since the ability to activate alkane C-H bonds under mild conditions, particularly at an isolated site, can suppress extensive decomposition of the alkane. The potential for creating materials that can promote

challenging chemistries such as alkane functionalization has motivated us to pursue fundamental investigations of the surface chemistry of early transition metal SAAs.

Model Ti-Cu alloy surfaces are selected as a representative system for examining the surface chemistry of early transition metal SAAs. Metallic Ti is highly oxophilic and expected to be reactive toward a wide range of compounds, including alkanes as well as oxygenates. Additionally, Ti and Cu are miscible over the entire range of compositions at temperatures above about 200 °C and form several intermetallic compounds.[14-15] Consistent with the bulk phase behavior, prior studies show that Ti deposition onto Cu(111) at room temperature produces a disordered Ti overlayer, but that alloy formation can be induced by heating above 400 °C.[16] These findings suggest that Ti can atomically disperse into the Cu(111) surface, provided that kinetic barriers to intermixing can be overcome under conditions at which Ti is maintained in the surface layer.

In this study, we investigated the structural and CO binding properties of surfaces prepared by depositing small amounts of Ti onto Cu(111), aiming to identify conditions that enable the formation of a dilute surface alloy. Our results show that Ti containing islands partially capped with a Cu overlayer preferentially form on ascending step edges of Cu(111) below about 400 K while Ti alloying into the ascending steps becomes dominant during Ti deposition between ~500 and 600 K; islands formed on terraces at all temperatures studied. Measurements using RAIRS and DFT calculations demonstrate that CO gives rise to distinct C-O stretch bands when adsorbed on Cu-covered Ti containing domains vs. isolated Ti atoms in the Ti-Cu(111) surface alloy. This study confirms that a Ti-Cu(111) surface alloy with single atom sites can be generated by Ti deposition on Cu(111), thus affording opportunities for future investigations of the surface chemistry of Ti-Cu(111) SAAs.

Experimental Details

Scanning tunneling microscopy (STM) and reflection absorption infrared spectroscopy (RAIRS) measurements were performed in an ultrahigh vacuum (UHV) system described previously.[17] The UHV chamber is equipped with a scanning tunneling microscope (RHK), a four-grid retarding field analyzer (SPECS) for low-energy electron diffraction (LEED) and Auger electron spectroscopy (AES), a quadrupole mass spectrometer (QMS) (Hiden), a Fourier transform infrared spectrometer system (Bruker, Tensor 27), an ion sputter gun, and an electron-beam metal evaporator (McAllister Technical Services) for vapor deposition of Ti.

The Cu(111) crystal used in this study is a circular top-hat-shaped disk (10 mm × 1.65 mm) cut to isolate the (111) surface plane within a tolerance of ± 0.1°. Details of the sample support structure have been reported previously.[18] The Cu(111) sample was cleaned by repeated cycles of Ar^+ (2.0 keV, 0.2 μA) sputtering at 300 K followed by thermal annealing at 700 K. A low annealing temperature was used to increase the step density on the Cu(111) surface in an effort to enhance the dispersion of Ti into the Cu(111) surface due to the expected tendency for dopant metals to incorporate into step edges.[7,19-21] To prevent Ti oxidation from the background gas, oxygen was not introduced into the chamber during the course of these experiments. We considered the Cu(111) sample to be clean when Auger electron spectra exhibited no discernable signals for the C(KLL), S(KLL) and O(KLL) peaks and a sharp LEED pattern characteristic of Cu(111) was observed.

Metallic Ti was deposited onto the Cu(111) sample using a e-beam evaporator fitted with a Ti rod. Evaporation was performed in UHV with the sample held at constant temperatures between 300 and 700 K. AES spectra showed that negligible amounts of impurities, particularly C and O, were present on the sample after Ti deposition. The Ti coverage was estimated by

calculating the area covered by Ti islands observed in STM images acquired after depositing Ti below ~400 K. Because Ti island formation dominates at these temperatures (see below), we assume that the fractional area covered by the Ti islands is representative of the Ti coverage for low temperature deposition. From this analysis, we estimate an average Ti deposition rate of ~0.02 ML/min where 1 ML is defined as the surface atom density of Cu(111). Most of the data presented below was obtained after depositing ~0.04 ML of Ti.

STM measurements were performed at a sample temperature of ~300 K and the tunneling interaction was set to constant current feedback mode. The equipment used for STM was produced by RHK and includes a UHV 300 "beetle-type" scan head operated with an SPM 100 controller. Images were collected at typical scan settings in the range of +0.08 to +0.5 V sample bias and tunneling currents of 0.4–1.2 nA. Feature heights estimated from STM line scans were calibrated to the Cu(111) monatomic step height of 0.210 nm. RAIRS measurements were performed by reflecting a non-polarized IR beam from the sample at an incident angle of ~80° from the surface normal and detecting the reflected beam using an external, liquid-nitrogen cooled MCT detector. All of the reported RAIRS spectra are an average of 512 scans and were collected at 4 cm^{-1} resolution.

Computational Details

Density Functional Theory

Periodic density functional theoretical (DFT) calculations were completed using the Vienna ab initio Simulation Package (VASP).[22-25] Electronic exchange and correlation were described using the Perdew-Burke-Ernzenhof (PBE)[26] functional and electron-ion interactions are calculated with the projector-augmented-wave (PAW) method.[27-28] 3s and 3p electrons for Cu

and Ti were included in the core. The second-order Methfessel-Paxton scheme was employed for partial orbital occupancy near the Fermi-level, with a smearing of 0.2 eV, as is typical for metallic systems.[29] A dipole correction was applied to each supercell slab considered in this study, fixed to the center of mass, and van der Waals (vdW) dispersion corrections were applied to all calculations, employing the DFT-dDsC formalism such that the dispersion coefficients and damping function exhibit dependencies on the charge-density.[30-32] All calculations were spin-polarized. To adequately sample the Brillouin zone of the (3·3) supercell, a $5 \cdot 5 \cdot 1$ Monkhorst-Pack k-point mesh and a cutoff energy of 500 eV were employed for both the Cu(111) and Ti(0001) surfaces. The k-point mesh was decreased to $3 \cdot 3 \cdot 1$ only in the case of the Ti_7/Cu(111) island, which employed a $(6 \cdot 6)$ supercell, and was maintained at $5 \cdot 5 \cdot 1$ for the $(2\sqrt{3} \times 2\sqrt{3})$ unit cell of the rotated layered structure described below. Convergence criteria for all calculations were set to $1 \cdot 10^{-5}$ eV for the energies, and 0.02 eV/Å for the forces experienced by each atom that was allowed to relax.

Alloy Creation for CO Adsorption

In order to evaluate the potential influence of small clusters and ensembles of Ti on the experimental observations of both STM and RAIRS of adsorbed CO on Ti/Cu(111), alloys of various compositions and configurations were created. Supplementary Material (SM) describes the methods used to create supercells for the calculations (S1). The structures of immediate interest to the experimental results provided below are defined as: Ti_{island}/Cu(111), Ti_{ML}/Cu(111), Cu_{ML}/Ti_{ML}/Cu(111), $Cu_{ML}/Ti_{ML}R30°$/Cu(111), Ti_n-Cu(111) alloy and Cu_{ML}/Ti_n-Cu(111) subsurface alloy (Figure S1). Briefly, a 7-atom island of close-packed Ti atoms was created, using a $(6 \cdot 6)$ supercell of Cu(111) with 4 atomic layers. Ti_{ML}/Cu(111) denotes a pseudomorphic

monolayer of Ti on a (3 · 3) Cu(111) supercell, where the Ti atoms substitute the Cu in the lattice positions of the surface atomic layer, and $Cu_{ML}/Ti_{ML}/Cu(111)$ represents a layered structure in which a single, close-packed layer of Cu atoms is located on top of the $Ti_{ML}/Cu(111)$ structure. The close-packed Ti layers in these structures are highly strained (~16%) because the nearest neighbor distances in fcc Cu and hcp Ti differ significantly (a_{Cu111} = 2.55 Å and a_{Ti0001} = 2.95 Å). We find that a nearly unstrained Ti(0001)-Cu(111) interface can be generated by rotating one of the unit cells by 30° relative to the other; the ratio of close-packed distances is $a_{Cu111}/a_{Ti0001} \approx \sqrt{3}/2$ to within less than 0.2% and the rotated Ti(0001) single-layer would form a $(2\sqrt{3} \times 2\sqrt{3})R30°$ coincident unit cell in the Cu(111) basis (or a (3 × 3) in the Ti(0001) basis). Accordingly, for the model $Cu_{ML}/Ti_{ML}R30°/Cu(111)$ structure (Figure S1), the Ti(0001) subsurface layer is oriented 30° relative to the unit cells of both the surface and subsurface Cu(111) layers. Here, a $(2\sqrt{3} \times 2\sqrt{3})$ supercell was employed for our calculations. Although this rotation of the Ti layer eliminates lattice strain, it also lowers the coordination numbers of the Ti atoms with the adjacent Cu atoms. The Cu atoms at each Cu-Ti interface are positioned over top and bridge sites of the Ti(0001) layer since DFT predicts that this stacking sequence is energetically preferred. The two inequivalent Cu surface sites positioned over top and bridge sites of the Ti subsurface layer are denoted as Cu_*t* and Cu_*b*, respectively, and are present in a 1:3 ratio. Lastly, the single-atom alloy (SAA, n = 1) and other dilute surface alloys are denoted as Ti_n-Cu(111) using a (3 · 3) supercell, where Ti substitutes Cu atoms in the surface atomic layer. Dilute alloys created by placing close-packed arrangements of Ti atoms in the subsurface atomic layer are denoted by Cu_{ML}/Ti_n-Cu(111). As an example, the Cu_{ML}/Ti_3-Cu(111) structure is generated by replacing three Cu atoms in the Cu(111) subsurface with a triangular, close-packed Ti trimer. All atomic structures reported in this study were visualized using VESTA.[33]

CO Adsorption and Correlation Corrections

Following optimization of the various Ti_n-Cu(111) surfaces, CO was introduced to all plausible high-symmetry sites to determine energies of adsorption and vibrational frequencies. Vibrational frequencies were obtained from the Hessian matrix, which could be calculated using the finite difference method. Specifically, each ion is moved along the three cartesian directions through a small step size of ± 0.01Å. The matrix was subsequently computed from the forces. Throughout the course of this investigation, it became apparent that horizontal binding geometries were also likely for alloys containing Ti, so CO was introduced to each surface in both surface-normal and surface-parallel orientations. Binding energies of adsorbed CO were calculated using Equation (1),

$$E_b^{CO} = (E_{surf} + E_{CO}) - E_{surf}^{CO}$$

where E_{surf}^{CO} is the total energy of the surface bound CO system, E_{surf} is the total energy of the bare surface, and E_{CO} is the energy of CO in the gas-phase. The convention here is that positive energy means stable adsorption. Test calculations indicate that a (3 × 3) unit cell is adequate for accurately representing CO adsorbed on the model Ti_1-Cu(111) SAA as the CO binding energy on this structure differs by only 0.04 eV when computed using a (4 × 4) vs. (3 × 3) unit cell.

As has been described in detail previously,[34-35] GGA functionals such as the PBE+dDsC functional tend to overestimate the adsorption energy of CO on certain high-symmetry sites of metal surfaces, which leads to incorrect predictions for the lowest energy adsorption geometry. To account for this, each CO adsorption energy was corrected in the scheme discussed previously.[36-37] Briefly, the adsorption energy was calculated using five separate pseudopotentials with different core radii for both C and O (e.g., C_h, C_s, C_GW, and

C_GW_new). To account for the different accuracy requirements of each pseudopotential, the cutoff energy for each calculation was set to 1.2·ENMAX, except for _h, which employed a cutoff energy of 700 eV. Following optimization, energies of adsorption for each pseudopotential were plotted against the singlet-triplet electronic excitation of CO, denoted as $\Delta E_{S\text{-}T}^{CO}$, computed with the same pseudopotentials for C and O. The data were then fit with a linear regression and extrapolated to $\Delta E_{S\text{-}T}^{CO}$ = 6.095 eV,[38] which is the excitation energy value determined using coupled-cluster and configuration interaction calculations, which are comparable with the experimental value. From this treatment, the DFT method employed here is able to produce more accurate adsorption geometries and energies of adsorption for CO on a variety of Ti/Cu(111) and Cu/Ti(0001) surfaces.

Alloy Stability

In order to determine the enthalpic preference between Ti_n-Cu(111) alloys considered here, the chemical potential of Ti in each structure was calculated with reference to both bulk fcc-Cu and the bare Cu(111) surface. This was accomplished using Equation (2), given as

$$\mu_{Ti}\ (\text{eV/atom}) = (n_{Ti})^{-1} \cdot (E_{alloy\text{-}surf} - E_{Cu\text{-}surf} + \Delta N_{Cu} \cdot E_{bulk,Cu}) \quad (2)$$

where μ_{Ti} is the chemical potential of Ti in a given alloy, n_{Ti} is the number of Ti atoms, E_{alloy} is the total energy of the Ti/Cu alloy being considered, ΔN_{Cu} is the change in the number of Cu atoms relative to a stoichiometric Cu(111) surface of the same supercell dimensions, and $E_{bulk,Cu}$ is the bulk cohesive energy per atom of fcc-Cu. Bulk cohesive energies were determined from the bulk optimizations described above. By convention of the expression employed, a more negative chemical potential denotes relative preference for Ti to be incorporated into the Ti-Cu alloy being considered. These values were not referenced to bulk Ti, since the assumption that we have an available bulk of Ti to which these atoms could relocate is not necessarily valid. This

is further justified by experimental data being extracted in the dilute limit of Ti on Cu(111), but conclusions can still be made on the relative stability between structures.

In addition to chemical potential, the preference of Ti-ensembles in the Cu(111) surface to either aggregate into larger clusters, or segregate into the subsurface was assessed. Hence, Equations (3) and (4) were employed to determine aggregation and segregation, respectively, given by

$$E_{agg}\ (\text{eV/atom}) = (n_{Ti})^{-1} \cdot (E_{alloy\text{-}surf} + (n_{Ti} - 1) \cdot E_{Cu\text{-}surf} - n_{Ti} \cdot E_{SAA})$$

$$E_{seg}\ (\text{eV/atom}) = (n_{Ti})^{-1} \cdot (E_{SAA\text{-}surf} + E_{SAA\text{-}subsurf})$$

such that $E_{agg} > 0$ denotes a preference for isolation of the dopant atom, and $E_{seg} < 0$ denotes an enthalpic preference for the isolated SAA to remain in the surface atomic layer of the Cu(111) host.

Results and Discussion

Structure of Ti-Cu(111) surfaces

The surface morphological features observed with STM suggest that Ti alloying into the Cu(111) surface occurs to only a limited extent during Ti deposition at temperatures below about 400 K, with island formation dominating instead. As seen in Figure 1a, small islands with an average diameter of 3.5 ± 0.5 nm preferentially decorate ascending step edges after Ti deposition at 400 K (cluster size analysis; Figure S2), while larger islands with diameters ranging from 10 to 25 nm are dispersed on the terraces (Figure 1a,b). The small and large islands cover about 1.2% and 2.7% of the surface, respectively. The small islands have uniform heights of about 0.24 nm above the step edge, consistent with a single metal layer. Most of the large islands on terraces are irregularly shaped and consist of a single layer partially covered by a second layer for which the average heights are 0.25 and 0.20 nm, respectively (Figure S3). These heights are close to the

ideal layer separation in Ti(0001) and Cu(111) (0.234 vs. 0.210 nm), suggesting that these islands correspond to a single Ti-rich layer partially covered by a single Cu layer. Several of the bright, irregularly shaped islands are attached to smooth hexagonal islands (arrow, Figure 1), which are attributed to single-layer Cu(111) domains based on line-scan analysis (Figure S3). The formation of Cu(111) islands and their attachment to Ti-rich islands suggests that Cu atoms are sufficiently mobile to diffuse to the edges and top surfaces of the Ti-rich islands during Ti deposition at 400 K.

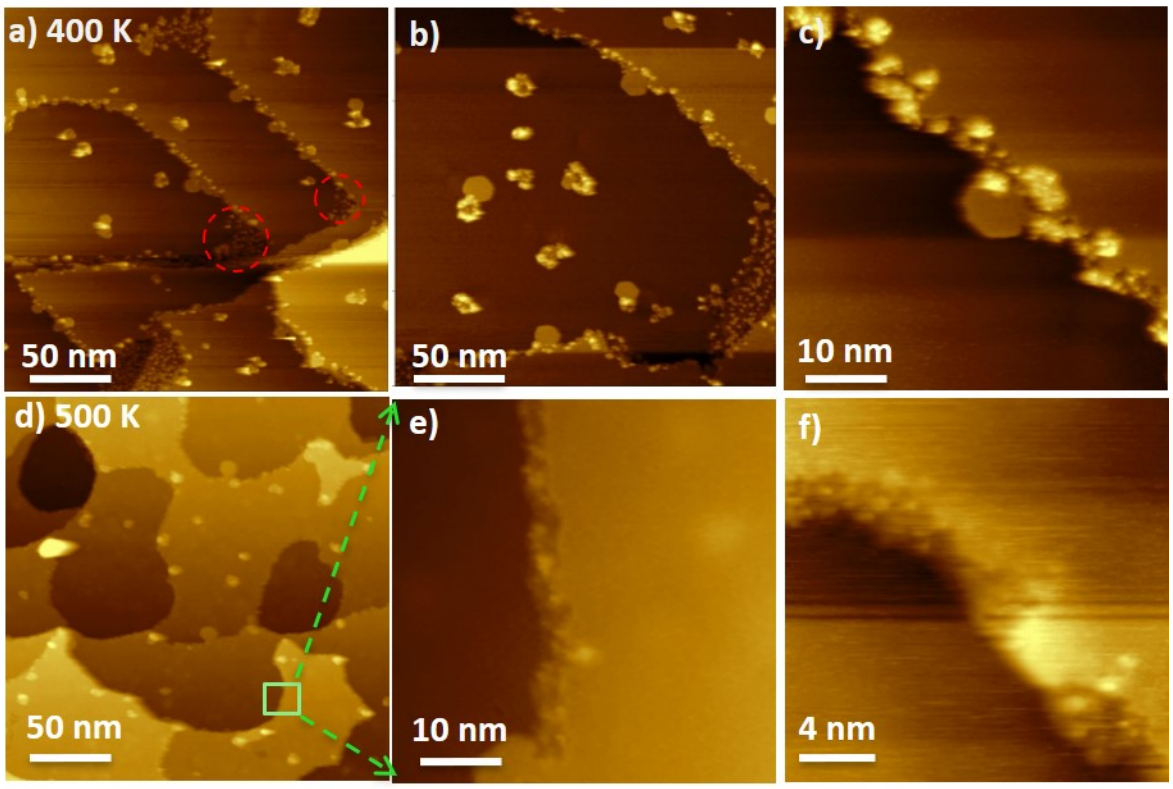

Figure 1. STM images of Ti-Cu(111) surfaces formed by deposition of Ti at different temperatures. a,b,c) 0.04 ML of Ti was deposited on Cu(111) at 400 K; d,e,f) 0.04 ML of Ti was deposited on Cu(111) at 500 K. Typical imaging conditions were 500 pA and 326 mV. The high resolution image in f) was collected using 0.58 nA and 302 mV imaging conditions. Groupings of Cu single layer islands are circled in red in a).

Magnified images further reveal that pits coexist with islands on the ascending step edges (Figure 1c), suggesting that restructuring occurs locally as islands form on the steps. The areas

covered by pits and islands at the step edges are similar. Several dense groupings of small islands (a few nm) are also evident at descending step edges (Figure 1a,b), with these regions extending from about 30 to 60 nm from the step edge. These islands generally have the same height as a monatomic step (0.21 nm) and are attributed to pure Cu that was ejected from the step edge during Ti deposition. The formation of islands on steps as well as the apparent release of Cu atoms from step edges suggests that alloying of Ti atoms into the Cu(111) surface occurred to a limited extent during deposition at 400 K.

Deposition of Ti at slightly elevated temperature promotes the formation of a Ti-Cu(111) alloy at the ascending step edges. After Ti deposition at 500 K, the small, bright islands observed at lower temperature are no longer evident in STM images and instead the brims of the ascending step edges exhibit darker contrast than the upper Cu(111) terraces (Figure 1d-f). Larger islands are still present on the terraces (Figure 1d) but dense groupings of single-layer Cu islands are absent on the lower terraces after Ti deposition at 500 K. The area covered by the large islands is the same as that estimated for the Ti-Cu(111) surface generated at 400 K. We attribute these changes in morphology to the formation of a Ti-Cu(111) alloy at the ascending step edges.

Our STM observations agree well with several studies which demonstrate a strong preference for alloy formation at the ascending step edges of Cu(111).[7,19-21,39] This prior work reveals that the dominant alloying mechanism occurs through place exchange between the dopant and host atoms as the dopant atoms impinge on ascending step edges, and produces alloy brims with higher concentrations of the dopant compared with the terraces. In contrast, dopant atoms tend to reflect from descending step edges. In agreement with these studies, we find that the ascending step edges on Cu(111) are preferentially modified by Ti. Our results provide evidence that alloying occurs predominantly at the steps during Ti deposition at elevated temperature (~500 to

600 K). However, Ti deposition at lower temperature mainly induces island formation on the ascending step edges and causes Cu atoms to release onto the terraces, suggesting that alloying is kinetically limited under these conditions.

The islands present on ascending steps are attributed to Cu-capped, Ti-rich regions within the step edge. This interpretation considers that Ti atoms incorporate into ascending steps by place exchanging with Cu atoms. At low temperature, kinetics appears to suppress alloying of Ti and Cu, and instead small, Ti-rich regions are produced within the step and the place-exchanged Cu atoms tend to migrate on top of these Ti atoms, resulting in Cu islands. The appearance of pits on the ascending steps is consistent with displacement of Cu and formation of Ti-rich regions within the step edges. As mentioned above, the larger, irregularly-shaped islands on the terraces are also attributed to Ti that is partially covered by Cu atoms, given that the height of the bottom layer is greater than the second layer. Significantly, the second layer of the large islands is an average height of 0.45 nm above the terrace and the small islands on step edges also rise ~0.45 nm above the lower terrace. This similarity supports the idea that both types of islands correspond to Cu-capped Ti-rich domains.

Since etch pits are not observed on the terraces, the Cu atoms covering the larger islands likely originate from the step edges. The significant span of the Cu island groupings away from the lower terraces as well as the formation of hexagonal islands attached to the Ti-rich islands suggests that Cu atoms released from the steps are sufficiently mobile at 400 K to reach Ti islands on the terraces. As discussed for other alloy systems,[7,39-40] the higher surface free energy of Ti (1.749 J/m^2) compared with Cu (1.566 J/m^2) provides a thermodynamic driving force for the capping of Ti domains by a Cu single layer.[41] In support of the proposed mechanism, prior studies have shown that a Ag capping-layer also tends to cover single-layer Pd islands on

Ag(111) at temperatures below that needed to induce PdAg alloy formation.[40] Below we present results of CO RAIRS measurements that further support the idea that a Cu capping layer develops on the Ti-rich islands on Cu(111).

Surface vibrational spectroscopy of adsorbed CO

Measurements using surface vibrational spectroscopy of adsorbed CO demonstrate that Ti deposition onto Cu(111) creates new sites for CO binding and that the bonding characteristics of these sites depends on the local structure. After saturating pure Cu(111) with CO at 100 K, RAIRS exhibits a single dominant peak at 2073 cm^{-1} (Figure 2a) that originates from CO adsorbed on atop sites of Cu(111), in good agreement with prior studies.[12,42-43] Small peaks near 1810-1830 cm^{-1} have been previously observed at high CO coverages and assigned to CO adsorbed on threefold hollow sites of Cu(111),[12] but such peaks were not detected in the present study. A second C-O stretch band at 2102 cm^{-1} from adsorbed CO becomes evident after depositing Ti onto the Cu(111) surface at 400 K (Figure 2b). This new peak is assigned to atop-CO adsorbed on the Cu-capped Ti-rich islands that are prevalent after Ti deposition at 400 K (Figure 1a-c). In support of this assignment, the intensity of the band at 2102 cm^{-1} scales with the Ti coverage and this peak is significantly smaller than the main peak from CO on pure Cu(111) in RAIR spectra acquired after CO saturation at 100 K (Figure S4).

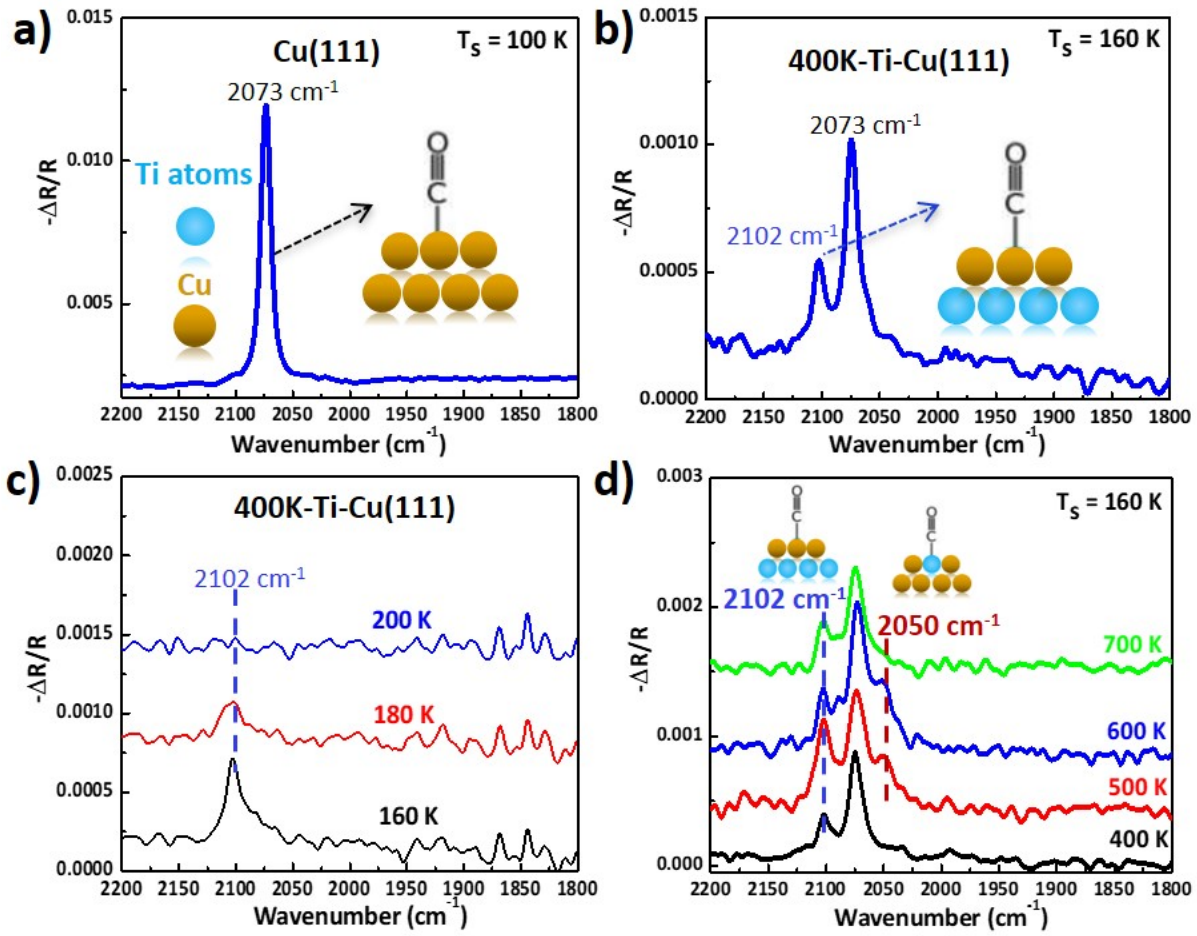

Figure 2. RAIRS spectra of CO adsorbed on pure and Ti-modified Cu(111). The spectra were acquired from the following surfaces and conditions: a) Pure Cu(111) after saturating with CO at 100 K and maintaining a CO background of 5×10^{-9} Torr. b) 0.04 ML Ti deposited on Cu(111) at 400 K after a 9 L CO exposure at 160 K and maintaining a CO background of 5×10^{-9} Torr. c) 0.04 ML Ti deposited on Cu(111) at 400 K after a 9 L CO exposure at 160 K, followed by evacuation of CO from the chamber and then heating in 20 K steps from 160 to 200 K. d) 0.04 ML Ti deposited on Cu(111) at temperatures of 400, 500, 600 and 700 K. Each surface was exposed to 9 L of CO at 160 K and held in a CO background of 5×10^{-9} Torr during data acquisition. A CO exposure of 9 L was found to saturate pure Cu(111) with CO at 100 K and establishes a steady state coverage(s) at 160 K on the Ti-modified surfaces.

The new CO species associated with Ti binds more strongly than CO on pure Cu(111). The RAIR spectrum shown in Figure 2b was acquired while the Ti-Cu(111) surface was held at 160 K in a CO background of 5×10^{-9} Torr. The peak at 2102 cm^{-1} was better resolved under these conditions because its intensity diminished more slowly with increasing temperature than the peak from CO on pure Cu(111). After evacuating CO from the chamber, the RAIRS peak for CO

on pure Cu(111) is no longer visible in spectra collected at 160 K while the peak at 2102 cm^{-1} is evident but diminished to the baseline after heating to 200 K (Figure 2c). This behavior demonstrates that the CO species associated with the Ti-containing islands achieves slightly stronger binding (~0.10-0.15 eV) compared with CO adsorbed on pure Cu(111).

The bonding characteristics attributed to CO on Cu-capped Ti-islands are analogous to those observed for CO adsorbed on ultrathin Cu films grown on the close-packed Ta(110) surface.[44] Because Ta and Ti are both early transition metals (Group IVB vs. VB), it is reasonable to expect that these metals would impart a similar influence on the binding and electronic properties of ultrathin Cu overlayers. This prior work reports that the C-O stretch band is blueshifted by 20 to 30 cm^{-1} and that the CO desorption temperature is about 40 K higher for CO adsorbed on an ~1 layer Cu film on Ta(110) compared with pure Cu(100). These differences in the CO bonding properties are quantitatively similar to our findings for CO adsorbed on pure vs. Ti-modified Cu(111), and thus further support our conclusion that the C-O stretch band at 2102 cm^{-1} originates from CO adsorbed on Ti-rich islands covered by a single Cu layer.

Similar to our observations for Cu-covered Ti-rich islands, undercoordinated sites on pure Cu surfaces also bind CO more strongly and cause the C-O stretch band of adsorbed CO to blueshift compared with CO on Cu(111) terraces. Prior studies of sputter-damaged Cu surfaces demonstrate that bands near 2090 and 2100 cm^{-1} arise from CO adsorbed on Cu sites with 7- to 8-fold vs. 6-fold coordination, respectively, where the latter coordinative environment is analogous to kink/corner sites or Cu_1 adatoms.[45-46] Similar low-coordination sites also form on Cu surfaces above about 300 K during exposure to elevated CO pressures (~0.1 Torr) due to CO-induced surface restructuring.[45-47] In UHV, however, the coverages of such low-coordination sites on pure Cu surfaces becomes negligible after heating to 500 K,[46] which is well below the

700 K annealing temperature employed in our experiments prior to Ti deposition. On the basis of these comparisons, the present results suggest that the binding properties of CO on Cu-covered Ti containing islands are similar to those of low-coordination Cu sites on pure Cu surfaces.

Depositing Ti on Cu(111) at slightly elevated temperatures produces a surface site with binding properties that are distinct from those of the Cu-capped Ti-rich islands. As seen in Figure 2d, the CO RAIR spectra acquired from Ti-Cu(111) surfaces generated between 500 and 600 K exhibit a peak at ~2050 cm^{-1} in addition to the peaks at 2102 and 2073 cm^{-1}. A small peak at 2090 cm^{-1} is also evident in the RAIRS spectrum obtained from the Ti-Cu(111) surface prepared at 600 K. The appearance of the 2050 cm^{-1} peak coincides with evidence of alloy formation at the ascending step edges from STM (Figure 1d-f). The peak at 2050 cm^{-1} is thus attributed to CO adsorbed on sites within this Ti-Cu alloy. RAIR spectra collected after stepwise heating suggest that the CO species associated with the Ti-Cu(111) alloy has a binding energy that is intermediate to CO on pure Cu(111) and Cu-capped Ti-rich islands (Figure S6); however, further work is needed to accurately assess the binding strengths of these CO species.

Although alloy formation eliminates Ti-rich islands at the step edges, such islands continue to form on terraces during deposition above 500 K. We thus conclude that CO adsorbed on these islands gives rise to the RAIRS peak at 2102 cm^{-1} observed after Ti deposition at elevated temperature. The small peak at 2090 cm^{-1} is also assigned to CO adsorbed on the Cu-capped Ti-rich islands, with the CO in a different bonding environment compared with the species that produces the 2102 cm^{-1} peak. Overall, the combination of RAIRS and STM provides strong evidence that a Ti-Cu(111) surface alloy forms during Ti deposition at moderate temperatures (~500 to 600 K) and demonstrates that adsorbed CO experiences distinct binding on sites of the alloy compared with pure Cu(111) or Cu-covered Ti-rich islands.

The RAIRS peak assigned to the Ti-Cu(111) surface alloy (2050 cm^{-1}) is no longer evident after Ti deposition above ~700 K (Figure 2c), suggesting that Ti atoms that incorporate into the step edges tend to migrate into the subsurface at sufficiently high temperature. In contrast, the peak at 2102 cm^{-1} persists in the RAIR spectra. Thus the Cu-capped Ti containing islands on terraces appear to remain stable up to higher temperatures than the Ti-Cu(111) surface alloy. These findings suggest that the ascending steps facilitate Ti dissolution into the subsurface in addition to promoting surface alloy formation. The higher stability of Ti-rich islands on terraces suggests that kinetics stabilizes these islands against decomposition and incorporation into the subsurface to temperatures of about 700 K.

Surface characterization using CO RAIRS also demonstrates that annealing Ti-Cu(111) surfaces prepared below 400 K is ineffective at inducing alloy formation. The CO RAIR spectra only exhibit peaks at 2073 and 2102 cm^{-1} after heating to temperatures between 500 and 700 K; the 2050 cm^{-1} peak does not emerge (Figure S5). This behavior suggests that small Ti-containing islands within the ascending steps are also stable against decomposition and dispersion into the Cu(111) step edge, once the islands have formed. We thus conclude that Ti-Cu(111) alloy formation is efficient during Ti vapor deposition at elevated temperature because individual Ti atoms are impingent on the ascending steps and have enough thermal energy to incorporate and disperse into the step edge under such conditions.

DFT calculations of CO on Ti-Cu(111) structures

DFT calculations were used to characterize the stability and CO binding properties of several Ti-Cu(111) structures in an effort to identify the types of structures that formed during the experiments. Among the Ti-Cu structures investigated (Figure S1), the Cu_{ML}/Ti_1-Cu(111) and

Cu_{ML}/Ti_3-Cu(111) subsurface alloys, in which Ti atoms are located in the first subsurface layer of Cu(111), are the most stable configurations (μ_{Ti} = -7.53 and -7.52 eV/atom, respectively). The layered Cu_{ML}/Ti_{ML}/Cu(111) structure is the next most stable, followed by the Cu_{ML}/Ti_{ML}*R*30°/Cu(111) structure with the corresponding Ti chemical potentials equal to -7.50 and -7.42 eV/atom, respectively (Table 1). Interestingly, the greater stability of the Cu_{ML}/Ti_{ML}/Cu(111) structure compared to the rotated version demonstrates that the compressive strain (~16%) in the subsurface Ti layer of this structure is less destabilizing than the lower Ti-Cu coordination realized in the nearly strain-free Cu_{ML}/Ti_{ML}*R*30°/Cu(111) structure. Our results also reveal a moderate enthalpic preference for Ti to reside in the Cu(111) subsurface as the chemical potential of a Ti atom is 0.21 eV/atom less stable when the Ti atom is substituted into the surface layer of Cu(111) rather than the subsurface layer.[5,48] Lastly, relative to the Cu_{ML}/Ti_1-Cu(111) structure, the aggregation energies are small but positive with values of 0.01 eV and 0.03 eV for the Cu_{ML}/Ti_3-Cu(111) and Cu_{ML}/Ti_{ML}/Cu(111) structures, respectively, indicating a slight enthalpic preference for subsurface Ti to disperse. Entropic gain will further enhance the thermodynamic driving force for Ti to mix into the Cu(111) subsurface. Thus, in agreement with our experimental observations, the DFT results predict a thermodynamic driving force for Cu atoms to migrate on top of Ti-containing islands that form during deposition onto Cu(111) and generally for Ti to reside in the subsurface.

Table 1. Chemical potential of Ti (μ_{Ti}) in Ti-Cu close-packed surface structures and bonding properties of adsorbed CO determined from DFT. Listed are the computed C-O stretch frequencies (ν_{CO}) for CO adsorbed on an atop site, the site and geometry of the most stable CO species on each surface and the corresponding binding energies of these CO species. The values in parentheses are experimental values of ν_{CO} for CO adsorbed on the structure to which the experimental band is attributed. Images of the Ti-Cu structures with an adsorbed CO molecule are shown in Figure S7. *C-O stretch frequencies and binding energies are shown in order for CO adsorbed on Cu_*t* and Cu_*b* sites, respectively. **The molecule was constrained to remain on the Cu top site to calculate the C-O stretch frequency of CO adsorbed on the Ti_1-Cu(111)-sub alloy.

Structure	μ_{Ti} (eV/atom)	Atop (cm^{-1})	Site and geometry of most stable CO species	Binding energy of the most stable CO species (eV)
Cu(111)	---	2048 (2073)	Atop; upright	0.75
Ti(0001)	---	1830	Hollow (fcc); flat-lying	2.33
Ti_{ML}*R*30°/Cu(111)	-7.10	---	---	---
Ti_{ML}/Cu(111)	-7.14	1870	Hollow (fcc); flat-lying	1.92
Ti_{island}/Cu(111)	-7.25	1885	Hollow (fcc); tilted	1.58
Ti_1-Cu(111) alloy	-7.32	1996 (2050)	Atop; upright	1.21
Ti_2-Cu(111) alloy	-7.32	---	Bridge; flat-lying	1.70
Ti_3-Cu(111) alloy	-7.32	---	Hollow (fcc); flat-lying	2.29
Cu_{ML}/Ti_{ML}*R*30°/Cu(111)*	-7.42	2042, 2011	Atop; upright	0.95, 0.83
Cu_{ML}/Ti_{ML}/Cu(111)	-7.50	2016	Atop; upright	0.73
Cu_{ML}/Ti_3-Cu(111)	-7.52	2068 (2102)	Atop; upright	0.86
Cu_{ML}/Ti_1-Cu(111)	-7.53	2043**	Hollow (fcc); upright	---

The surface Ti_1-Cu(111) alloy has the highest stability among the structures studied with Ti atoms located at the surface. Similar to the Ti subsurface structures, Ti_{ML}*R*30°/Cu(111) is the least stable, followed by the Ti_{ML}/Cu(111) structure. The pseudomorphic Ti island on Cu(111) is more stable than a complete Ti layer because the island expands to alleviate lattice strain, yet the surface alloys are more stable than the pure Ti island by about 0.07 eV/atom. Relative to the Ti_1-Cu(111) surface alloy, the aggregation energies are only slightly positive (< 0.01 eV) for the surface Ti dimer and trimer alloys, the latter structure being represented by a triangular arrangement of close-packed titanium atoms (see SM Figure S1). This finding demonstrates that the enthalpic driving force for Ti aggregation within the Cu(111) surface layer is negligible, and thus suggests that Ti_1-Cu(111) surface moieties are favored over larger ensembles due to the gain in configurational entropy that would result from Ti dispersion into the surface.

Overall, the relative stabilities determined from DFT support our assignments of the Ti-Cu structures observed experimentally and provide key insights for understanding the

thermodynamics governing their formation. It is important to recognize, however, that kinetics can play an important role in determining the types of structures that form, depending on conditions. For example, our experimental results suggest that kinetic barriers stabilize Ti atoms in the Cu(111) surface layer at temperatures up to ~600 K, even though subsurface Ti is more stable. Additionally, as observed for other systems,[48-50] it is reasonable to expect that the surface segregation of Ti atoms can be induced by adsorbing compounds at sufficient partial pressures and temperatures, particularly considering that the segregation energy is only ~0.2 eV. Ultimately, additional studies are needed to determine the mechanisms for Ti alloying into Cu(111) and the conditions at which meta-stable surface structures remain kinetically trapped and are thus available to promote surface chemical reactions.

Our calculations of CO binding properties further support our assignments of the surface structures that form during Ti deposition on Cu(111). The calculations predict that CO, after adsorption energy correction as described, preferentially adsorbs on atop sites of Cu(111) and that this atop-CO species has a binding energy of 0.75 eV and a C-O stretch frequency of 2048 cm^{-1} (Table 1). Comparison with experimental data shows that the DFT calculations slightly overestimate the CO binding energy (~0.5 eV) and underestimate the C-O stretch frequency on Cu(111) (2073 cm^{-1}).[43,51-52] However, we expect that differences in the CO binding properties among various Ti-Cu(111) structures will be more accurately represented by our calculations so we focus on making comparisons rather than assessing the absolute values of the binding energies and stretch frequencies.

According to DFT, CO preferentially adopts flat-lying geometries on contiguous Ti surface ensembles with more than one Ti atom and binds markedly more strongly than CO on pure Cu(111). For example, at low coverage CO achieves optimal binding on Ti(0001) by adsorbing

on an fcc hollow site and aligning its bond axis nearly parallel to the surface plane (Figure S7). The binding energy for this configuration is about 2.33 eV (Table 1), which is significantly higher than that computed for CO on pure Cu(111) (0.75 eV). The calculations also predict that CO preferentially lies nearly flat on other close-packed Ti moieties, including a Ti single-layer on Cu(111) (Table 1) as well as a Ti dimer and trimer substituted into the Cu(111) surface (Figure S7). In general, flat-lying CO species would be undetectable in RAIRS due to the surface dipole selection rule.[53] Therefore, the DFT results suggest that even if contiguous Ti surface domains are formed, they may not be identifiable using CO RAIRS.

We also computed C-O stretch frequencies for upright geometries of CO adsorbed on top sites of Ti atoms in several contiguous Ti surface ensembles, given the possibility that such adsorbate geometries may form at the high CO coverages probed experimentally. The C-O stretch frequencies of these atop-CO species are predicted to lie in a range from 1830 to 1885 cm^{-1} (Table 1, Figure S7). Our RAIR spectra do not exhibit discernible C-O stretch bands in this range ($<\sim$ 2000 cm^{-1}), therefore suggesting that atop-CO species either do not form on contiguous Ti surface domains or that such domains are not present on the surface. As shown above, STM images provide evidence that a large fraction of the Cu-capped Ti-rich islands which form on terraces expose areas with pure Ti (Figure 1). Thus, based on the absence of RAIRS peaks below 2000 cm^{-1}, we conclude that CO would preferentially adsorb into flat-lying rather than upright geometries if contiguous Ti surface ensembles were present on the Ti-Cu(111) surfaces and thus would be undetectable by RAIRS. A key implication is that the new CO RAIRS peaks that emerge after Ti deposition onto Cu(111) are not associated with CO adsorbed on contiguous Ti surface ensembles.

The dissociation of CO on contiguous Ti surface domains would also eliminate RAIRS peaks from CO initially adsorbed on such structures but dissociation is expected to occur negligibly at the low temperatures (~160 K) at which the CO RAIRS experiments were performed. Prior studies report that CO dissociation does occur extensively on Ti(0001) at about 300 K.[54] However, we estimate from DFT that the CO dissociation barrier is about 0.66 eV on single-layer Ti/Cu(111) structures so the dissociation rate would be negligible below about 200 K (SM S9). Upon heating, however, CO dissociation on contiguous Ti surface structures should dominate over desorption because the dissociation barrier (~0.7 eV) is much smaller than the CO binding energies (>1.5 eV). Future experiments are required to determine if CO dissociation occurs on Ti-Cu(111) structures during heating.

The DFT results strongly suggest that the new redshifted C-O stretch band observed with RAIRS arises from CO adsorbed on isolated Ti atoms of a Ti-Cu(111) surface alloy (Figure 3a). The calculations predict that CO preferentially adsorbs in an upright geometry on the top site of a single Ti atom substituted into Cu(111) and that the CO molecule has a stretch frequency of 1996 cm^{-1} (Table 1), which is 56 cm^{-1} lower than the frequency of the experimentally observed band at 2050 cm^{-1}. DFT also predicts that the binding energy is higher for CO adsorbed on an isolated Ti site compared with pure Cu(111) (1.21 vs. 0.75 eV, Table 1), in qualitative agreement with our experimental observations (Figure S6). The computed C-O stretch frequency for the CO-Ti_1 species is significantly higher than the frequencies computed for atop-CO adsorbed on contiguous Ti surface structures (Table 1), and reasonably close in value to the experimentally observed band at 2050 cm^{-1} that is associated with the Ti-Cu(111) surface alloy. We thus conclude that the experimental band at 2050 cm^{-1} arises from CO adsorbed on isolated Ti atoms in the Ti-Cu(111) surface alloy.

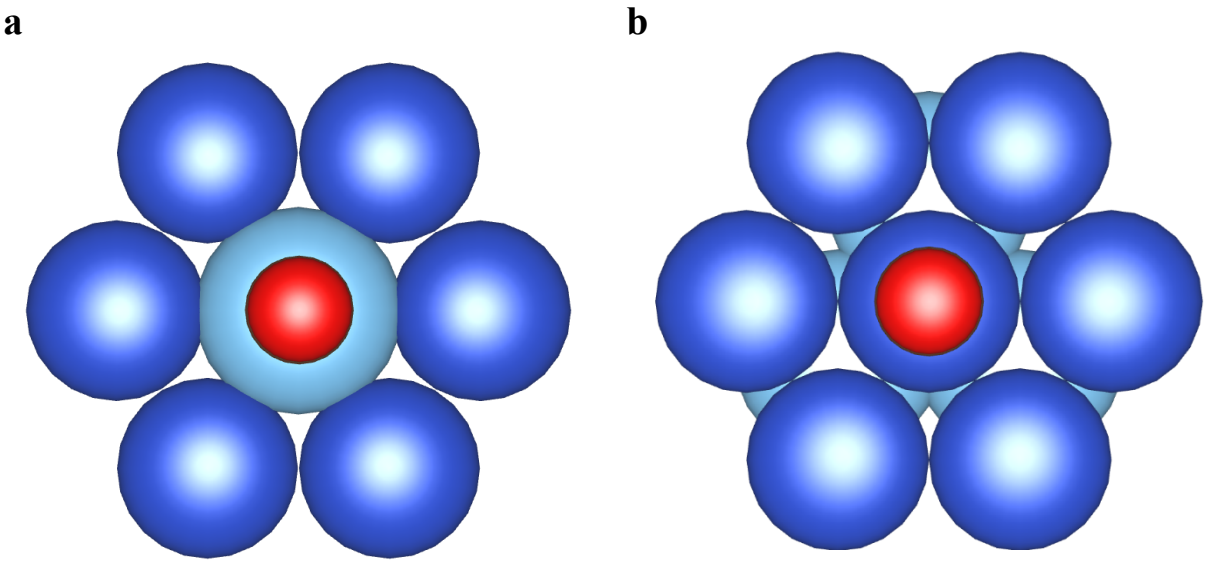

Figure 3. Models of CO adsorbed on a) a Ti atom of the Ti_1-Cu(111) surface alloy and b) a Cu atom of the Cu_{ML}/Ti_3-Cu(111) subsurface alloy. The CO molecule adopts an upright adsorption configuration, with the C atom closer to the metal surface. The Cu, Ti, C and O atoms are shown in blue, light blue, brown and red.

Our calculations show that the binding properties of CO on the Cu_{ML}/Ti_3-Cu(111) structure are similar to those identified experimentally for the Cu-covered Ti containing islands. For the Cu_{ML}/Ti_3-Cu(111) subsurface alloy, a surface Cu atom is located directly above the center of a close-packed arrangement of three Ti-atoms in the second layer (Figure S1). According to DFT, a CO molecule is stable in an upright configuration on top of this Cu site and has a binding energy of 0.86 eV and a C-O stretch frequency of 2068 cm^{-1} (Figure 3b). We also investigated CO adsorption on the Cu_{ML}/Ti_1-Cu(111) subsurface alloy but were unable to locate a local minimum for CO adsorption at the top sites of Cu atoms located close to the subsurface Ti monomer, making the correction procedure impractical. A calculation constraining the C atom laterally on top of these Cu atoms provided a CO stretch frequency of 2043 cm^{-1}, which is close to that computed for CO on pure Cu(111). For the Cu_{ML}/Ti_3-Cu(111) subsurface alloy, the CO binding energy is slightly higher (~0.13 eV) and the C-O stretch frequency is blueshifted by 20 cm^{-1} compared with pure Cu(111). These differences in the binding properties predicted for CO

on Cu_{ML}/Ti_3-Cu(111) vs. pure Cu(111) agree well with the differences that we measured experimentally. Specifically, our experimental data shows that the binding energy and the C-O stretch frequency are greater by ~0.1 to 0.15 eV and 29 cm^{-1} (2102 – 2073 cm^{-1}), respectively, for CO adsorbed on Cu-covered Ti-rich islands vs. pure Cu(111). We thus conclude that the binding properties of CO on the Cu-covered islands relative to the Cu(111) host surface are accurately reproduced by the model Cu_{ML}/Ti_3-Cu(111) structure.

The computed binding properties of CO adsorbed on layered Cu/Ti/Cu(111) structures, particularly the C-O stretch frequency, are sensitive to the geometric structure and composition of the subsurface layer (Table 1). For example, a Cu surface atom is positioned above a threefold Ti hollow site on both the Cu_{ML}/Ti_3-Cu(111) and Cu_{ML}/Ti_{ML}/Cu(111) structures, yet the C-O stretch frequencies of CO adsorbed on these Cu top sites are predicted to differ by more than 50 cm^{-1}; the frequencies are 2068 and 2016 cm^{-1} for CO on Cu_{ML}/Ti_3-Cu(111) and Cu_{ML}/Ti_{ML}/Cu(111), respectively. Similarly, the C-O stretch frequencies predicted for CO adsorbed on the Cu_*t* and Cu_*b* sites of the $Cu_{ML}/Ti_{ML}R30$/Cu(111) structure (Figure S1) are different from both one another (2042 vs. 2011 cm^{-1}) and those computed for CO on the non-rotated, subsurface layers. These results demonstrate that the bonding properties of the surface Cu atoms depend on the local concentration of the subsurface Ti as well as the geometrical arrangement of the Ti relative to the Cu surface. For example, the difference in Ti concentration between the Cu_{ML}/Ti_3 and Cu_{ML}/Ti_{ML} structures may cause a difference in charge transfer between the Ti and surface Cu and thus the CO binding (S10, SM). Differences in the local geometry and strain may also influence the surface bonding properties; for example, the in-plane Ti-Ti spacings in the Cu_{ML}/Ti_3 structure are about 4.5% larger than in the Cu_{ML}/Ti_{ML} structure (2.68 vs. 2.56 Å), approaching those of the model Ti island. Considering these computational

results, we suggest that the experimentally observed C-O stretch bands at 2102 and 2090 cm^{-1} originate from CO adsorbed on Cu atoms with different local structure and/or composition of the subsurface Ti in islands. Further study will be needed to assign the observed bands to CO adsorbed on specific Cu-Ti moieties.

Similar to the results for the CO-Ti_1 species, the computed C-O stretch frequency for CO on the Cu_{ML}/Ti_3-Cu(111) subsurface alloy is lower than the main experimentally observed band (by ~35 cm^{-1}). Several factors could be responsible for the differences between the computed and experimental frequencies, including effects of CO coverage, anharmonicity and inaccuracy in the computed bonding properties of the Ti-Cu structures. The CO coverage appears to have a negligible influence on the C-O stretch frequencies of CO adsorbed on the Cu-covered Ti-rich islands as the RAIRS peaks associated with this species do not shift appreciably as the CO coverage is decreased (Figure 2c). The discrepancy is thus more consistent with error in the computational modeling of the electronic properties of the Ti-Cu structures and/or the vibrational motion of adsorbed CO. Determining the origin of quantitative difference(s) between computed and experimental properties for the Ti-Cu structures will require further study and additional data, for example with experimental determination of adsorption energies and exploration of the sensitivity of calculated data with the choice of exchange correlation functional.

One should recall that DFT calculated adsorption energies present a general error of ~0.2 eV due to approximations in the exchange-correlation functional, so that quantitative agreement with experiments is by consequence limited. CO adsorption on transition metal surfaces is a case where significant overbinding from DFT exchange correlation functionals has been reported[55-56] and even after the adsorption energy correction developed here some overbinding remains (~0.2 eV for CO on Cu(111), for example). These proposed further studies lie outside of the scope of

the current work. However, our DFT predictions of the stability and CO binding properties of various Ti-Cu structures on Cu(111) provides good qualitative agreement with our experimental observations and provide insights into the fundamental origins of these properties. This concerns the relative CO frequencies between structures, for example, the difference of the CO stretch between the Ti_1 SAA structure and the Cu covered Ti-rich island (72 cm^{-1} in the calculation and 52 cm^{-1} in the experiment, see Table 1) and the relative adsorption energy of CO on the Cu covered Ti-rich island with respect to Cu(111), stronger by 0.10-0.15 eV in the experiment and by 0.10-0.20 eV in the calculated data.

Discussion

The DFT results support our assignments of the CO RAIRS peaks and thus the existence of the surface structures that give rise to these peaks, namely, isolated Ti atoms in the Ti-Cu(111) alloy and Cu-capped Ti-rich islands. The calculations also suggest that surface structures containing two or more neighboring Ti atoms would be undetectable with CO RAIRS due to the preference for CO to adopt flat-lying geometries on such structures. As an example, STM line scans provide evidence that contiguous surface domains of Ti are present on the Ti-rich islands which form on the Cu(111) terraces (Figure S3b), yet the RAIRS peaks that were detected are inconsistent with CO adsorbed on such Ti surface sites.

The preference for CO to adsorb in flat-lying geometries on contiguous Ti surface structures is distinct from the behavior of CO adsorbed on dilute alloys of Cu(111) with late transition metals (e.g., Ni, Rh, Pd, Pt),[9,12,57] and has consequences for characterizing Ti-Cu(111) surface alloys. For late transition metal dopants, CO adsorbs into an upright geometry irrespective of the metal ensemble size and exhibits a change in site preference from atop to bridge for isolated

dopant atoms vs. larger ensembles. Because the CO adsorption geometry remains upright, the change in site preference produces well separated C-O stretch bands in RAIRS that may be used to identify the presence of monomers vs. dimers of the minority metal component.[9,12,57] Our results suggest that an analogous characterization of Ti ensembles in the Ti-Cu(111) alloy is less feasible using CO RAIRS. We thus emphasize that our CO RAIRS results do not provide direct information about Ti dimers or larger ensembles that may be present in the Ti-Cu(111) alloy and that other characterization methods (e.g., low temperature STM) or probe molecules are needed to identify such structures and quantify their concentrations. Significantly, however, the preference for CO to adopt flat-lying geometries on contiguous Ti surface structures suggests that the CO RAIRS peak at 2050 cm^{-1} is an unique spectroscopic signature for isolated Ti sites in the Ti-Cu(111) surface alloys. Notably, our results show that the single-atom alloy co-exists with Cu-covered Ti containing islands for the Ti coverage (~0.04 ML) studied in this work. Depositing smaller amounts of Ti may limit the formation of islands on the terraces and enable the synthesis of surfaces with only the single atom Ti-Cu(111) alloy. Future studies should explore this possibility because the ability to generate only the SAA would facilitate experiments aimed at distinguishing the chemistry promoted by the SAA vs. Cu-covered Ti containing structures.

Although the CO RAIR spectra do not enable identification of contiguous Ti surface ensembles, our DFT calculations suggest that Ti monomers will be the most prevalent type of Ti ensemble in the surface alloy for the Ti coverage(s) studied. As discussed above, the DFT calculations predict negligible enthalpic differences among Ti monomers, dimers and trimers in Ti-Cu(111) surface alloys (Figure S1) and thus suggest that the larger entropic gain associated with Ti mixing into the surface layer will favor the formation of Ti monomers over larger

ensembles, at least at low Ti coverage. The intensity of the band attributed to CO on isolated Ti sites is comparable to that for CO on Cu-capped Ti-rich islands (Figure 2d), consistent with the idea that Ti monomers are the dominant type of Ti ensemble present in the surface alloys that were studied.

According to DFT, the bonding properties are quite distinct for the Ti atom in the Ti_1-Cu(111) surface alloy compared with a surface atom of Ti(0001). In particular, the calculations predict that the C-O stretch frequency is more than 160 cm^{-1} higher for CO adsorbed in an upright geometry on the Ti_1-Cu(111) site compared with a top site of Ti(0001) (Table 1). Notably, CO preferentially adopts a flat-lying geometry on Ti(0001) (Figure S7) so CO adsorbed on a top site of Ti(0001) represents a local minimum in the potential energy surface. Much smaller differences in the C-O stretch frequency, typically within 30 cm^{-1}, are observed for CO adsorbed on late transition-metal dopants in Cu(111) compared with close-packed surfaces of these metals.[9,12,58] Calculations of the pDOS demonstrate that the *d*-states projected onto a surface Ti atom are strongly modified when the Ti atom is substituted into the Cu(111) surface compared with Ti(0001) (SM, S10). Upon formation of the Ti_1-Cu(111) surface alloy, the *d*-band of the Ti-dopant narrows in width relative to the reference Ti(0001) surface, and a sharp peak emerges just above the Fermi level while the density of filled states near the Fermi level decreases (Figure S10). The higher C-O stretch frequency computed for atop-CO on the Ti_1-Cu(111) surface compared with Ti(0001) may arise from diminished π-backdonation resulting from the lower density of filled *d*-states at the Ti_1 site. The upshift in the *d*-band is attributed to charge transfer from the Ti atom to the Cu(111) substrate, which is mediated by the differences in electronegativity between Cu and Ti; the Pauling electronegativities are 1.90 and 1.54 for Cu and Ti, respectively.

This qualitative intuition is confirmed by the Hirshfeld charge analysis for this system, where the charge of Ti embedded in the Cu lattice obtained a value of +0.17 *e*, while the nearest-neighbor Cu atoms incur an average partial negative charge of -0.03 *e*. Hence, this demonstrates a small net-movement of electron density from Ti to Cu in the vicinity of the SAA. This result differs from those determined previously via analysis of bulk TiCu alloys and epitaxial thin-films by Vahakangas et al.,[16] where it was demonstrated that charge transfer could be explained via the empty states of each metal, meaning that net charge transfer was postulated as originating from the metal with the lower density of unoccupied states near the Fermi-level to the metal with a higher density of unoccupied states (e.g., Cu to Ti). There, it was determined that the surface states were dependent upon the coordination of Ti, whether it be adsorbed in an epitaxial layer, or incorporated in the Cu(111) lattice as a bulk alloy, and it was concluded that surface states were transferred from Cu to Ti. It must be noted, however, that these systems cannot be directly compared, as thin films and bulk alloys will have much different electronic structures than that for a SAA. Overall, these results demonstrate that isolation in the Cu(111) surface significantly modifies the electronic and bonding properties of Ti atoms relative to Ti(0001), and potentially produces a single atom alloy with unique chemical properties.

Summary

The structural and CO binding properties of Ti-Cu(111) surfaces were investigated as a function of the surface temperature during Ti deposition on Cu(111) using STM, CO RAIRS and DFT calculations. Our results show that small Ti containing islands covered by a Cu single layer preferentially form at ascending step edges during deposition below ~400 K, but that these islands are completely replaced by a Ti-Cu(111) surface alloy during Ti deposition between 500

and 600 K, with the alloying producing a brim at ascending step edges similar to other dilute alloys of Cu(111). Larger partially Cu-covered Ti containing islands were also dispersed on terraces after Ti deposition at all temperatures studied (~300 to 700 K). Surface alloy formation could not be induced by annealing as high as 700 K after Ti-rich islands were generated at step edges during deposition below 400 K, demonstrating that these islands are relatively stable against decomposition once formed.

Measurements using RAIRS of adsorbed CO show that a C-O stretch band at 2102 cm^{-1} originates from CO adsorbed on Cu-covered Ti containing islands, while a band at 2050 cm^{-1} is associated with CO adsorbed on sites within the Ti-Cu(111) single atom surface alloy. DFT calculations support these assignments as they predict that CO preferentially adsorbs on top sites of Cu above subsurface Ti ensembles and on top of an isolated Ti atom in a Ti-Cu(111) surface alloy and that the corresponding C-O stretch frequencies of these species differ by a similar amount as the experimentally observed bands. DFT further predicts that CO preferentially adsorbs in flat-lying geometries on contiguous Ti surface structures with more than one Ti atom and thus that CO adsorbed on such structures should be undetectable by RAIRS. These results demonstrate that a single atom Ti-Cu(111) alloy can be generated by depositing Ti on Cu(111) at slightly elevated temperature and that the alloy formation can be confirmed using CO RAIRS. The ability to generate a single atom Ti-Cu(111) alloy will provide opportunities to pursue experimental studies of a model early transition metal SAA and characterize surface chemistry promoted by this class of materials.

Supplementary Material

See the supplementary material for Supercell creation; Model Ti-Cu structures and stability; Cluster size distribution analysis; STM line scan analysis; Effect of the Ti coverage generated at 400 K on CO RAIRS; Effect of heating after Ti deposition at 300 K; CO RAIRS heating series after Ti deposition at 600 K; Images of CO adsorbed on model Ti-Cu structures; CO dissociation barrier on Ti/Cu(111); Projected density of states

Acknowledgements

This work was supported as part of the Integrated Mesoscale Architectures for Sustainable Catalysis, an Energy Frontier Research Center funded by the U.S. Department of Energy, Office of Science, Basic Energy Sciences under Award No. DE-SC0012573. C. J. O. acknowledges support by the National Science Foundation Graduate Research Fellowship Program under Grant No. (DGE1745303). C.J.O used the Odyssey cluster, FAS Division of Science, Research Computing Group at Harvard University. The calculations by H.T.N. were performed on the Hoffman2 cluster at UCLA Institute for Digital Research and Education (IDRE), and National Energy Research Scientific Computing Center (NERSC) of the U.S. Department of Energy. The authors are grateful to Prof. Charles Sykes for helpful discussions about single atom alloys.

Data availability

The data that support the findings of this study are available from the corresponding authors upon reasonable request.

References

1. Giannakakis, G.; Flytzani-Stephanopoulos, M.; Sykes, E. C. H., Single-Atom Alloys as a Reductionist Approach to the Rational Design of Heterogeneous Catalysts. *Acc. Chem. Res.* **2019**, *52*, 237-247.
2. Hannagan, R. T.; Giannakakis, G.; Flytzani-Stephanopoulos, M.; Sykes, E. C. H., Single-atom alloy catalysts. *Chem. Rev.* **2020**, *120*, 12044–12088.
3. Greiner, M. T.; Jones, T. E.; Beeg, S.; Zwiener, L.; Scherzer, M.; Girgsdies, F.; Piccinin, S.; Armbruster, M.; Knop-Gericke, A.; Schlogl, R., Free-atom-like d states in single-atom alloy catalysts. *Nature Chem.* **2018**, *10*, 1008-1015.
4. Fung, V.; Hu, G. X.; Sumpter, B., Electronic band contraction induced low temperature methane activation on metal alloys. *J. Mater. Chem. A* **2020**, *8*, 6057-6066.
5. Darby, M. T.; Stamatakis, M.; Michaelides, A.; Sykes, E. C. H., Lonely Atoms with Special Gifts: Breaking Linear Scaling Relationships in Heterogeneous Catalysis with Single-Atom Alloys. *J. Phys. Chem. Lett.* **2018**, *9*, 5636-5646.
6. Marcinkowski, M. D.; Darby, M. T.; Liu, J. L.; Wimble, J. M.; Lucci, F. R.; Lee, S.; Michaelides, A.; Flytzani-Stephanopoulos, M.; Stamatakis, M.; Sykes, E. C. H., Pt/Cu single-atom alloys as coke-resistant catalysts for efficient C-H activation. *Nature Chem.* **2018**, *10*, 325-332.
7. Lucci, F. R.; Lawton, T. J.; Pronschinske, A.; Sykes, E. C. H., Atomic Scale Surface Structure of Pt/Cu(111) Surface Alloys. *J. Phys. Chem. C* **2014**, *118*, 3015-3022.
8. Lucci, F. R.; Liu, J. L.; Marcinkowski, M. D.; Yang, M.; Allard, L. F.; Flytzani-Stephanopoulos, M.; Sykes, E. C. H., Selective hydrogenation of 1,3-butadiene on platinum-copper alloys at the single-atom limit. *Nat. Commun.* **2015**, *6*.
9. Hannagan, R. T.; Patel, D. A.; Cramer, L. A.; Schilling, A. C.; Ryan, P. T. P.; Larson, A. M.; Cinar, V.; Wang, Y. C.; Balema, T. A.; Sykes, E. C. H., Combining STM, RAIRS and TPD to Decipher the Dispersion and Interactions Between Active Sites in RhCu Single-Atom Alloys. *Chemcatchem* **2020**, *12*, 488-493.
10. Therrien, A. J.; Hensley, A. J. R.; Marcinkowski, M. D.; Zhang, R. Q.; Lucci, F. R.; Coughlin, B.; Schilling, A. C.; McEwen, J. S.; Sykes, E. C. H., An atomic-scale view of single-site Pt catalysis for low-temperature CO oxidation. *Nature Catalysis* **2018**, *1*, 192-198.
11. Cao, X. R.; Ji, Y. F.; Luo, Y., Dehydrogenation of Propane to Propylene by a Pd/Cu Single-Atom Catalyst: Insight from First-Principles Calculations. *J. Phys. Chem. C* **2015**, *119*, 1016-1023.
12. Kruppe, C. M.; Krooswyk, J. D.; Trenary, M., Polarization-Dependent Infrared Spectroscopy of Adsorbed Carbon Monoxide To Probe the Surface of a Pd/Cu(111) Single-Atom Alloy. *J. Phys. Chem. C* **2017**, *121*, 9361-9369.
13. Luneau, M.; Lim, J. S.; Patel, D. A.; Sykes, E. C. H.; Friend, C. M.; Sautet, P., Guidelines to Achieving High Selectivity for the Hydrogenation of alpha,beta-Unsaturated Aldehydes with Bimetallic and Dilute Alloy Catalysts: A Review. *Chem. Rev.* **2020**, *120*, 12834-12872.
14. Zhan, Y. Z.; Peng, D.; She, J., Phase Equilibria of the Cu-Ti-Er System at 773 K (500 ^{o}C) and Stability of the $CuTi_3$ Phase. *Metall. Mater. Trans. A* **2012**, *43a*, 4015-4022.
15. Zhu, Y. D.; Yan, M. F.; Zhang, Y. X.; Zhang, C. S., First-principles investigation of structural, mechanical and electronic properties for Cu-Ti intermetallics. *Comp. Mater. Sci.* **2016**, *123*, 70-78.
16. Vahakangas, J.; Williams, E. D.; Park, R. L., Surface-States in the Epitaxial-Growth of Titanium on Copper (111). *Phys. Rev. B* **1986**, *33*, 2281-2285.
17. Zhang, F.; Pan, L.; Li, T.; Diulus, J.; Asthagiri, A.; Weaver, J. F., CO oxidation on PdO(101) during temperature programmed reaction spectroscopy: Role of oxygen vacancies. *J. Phys. Chem. C* **2014**, *118*, 28647–28661.
18. Mehar, V.; O'Connor, C. R.; Egle, T.; Karatok, M.; Madix, R. J.; Friend, C. M.; Weaver, J. F., Growth and auto-oxidation of Pd on single-layer AgO_x/Ag(111). *Phys. Chem. Chem. Phys.* **2020**, *22*, 6202-6209.
19. Bellisario, D. O.; Han, J. W.; Tierney, H. L.; Baber, A. E.; Sholl, D. S.; Sykes, E. C. H., Importance of Kinetics in Surface Alloying: A Comparison of the Diffusion Pathways of Pd and Ag Atoms on Cu(111). *J. Phys. Chem. C* **2009**, *113*, 12863-12869.
20. Wang, Y. C.; Papanikolaou, K. G.; Hannagan, R. T.; Patel, D. A.; Balema, T. A.; Cramer, L. A.; Kress, P. L.; Stamatakis, M.; Sykes, E. C. H., Surface facet dependence of competing alloying mechanisms. *J. Chem. Phys.* **2020**, *153*.
21. Aaen, A. B.; Laegsgaard, E.; Ruban, A. V.; Stensgaard, I., Submonolayer growth of Pd on Cu(111) studied by scanning tunneling microscopy. *Surf. Sci.* **1998**, *408*, 43-56.

22. Kresse, G.; Hafner, J., Ab-initio molecular-dynamics simulation of the liquid-metal amorphous-semiconductor transition in germanium. *Phys. Rev. B* **1994**, *49*, 14251-14269.
23. Kresse, G.; Furthmuller, J., Efficient iterative schemes for ab initio total-energy calculations using a plane-wave basis set. *Phys. Rev. B* **1996**, *54*, 11169-11186.
24. Kresse, G.; Furthmuller, J., Efficiency of ab-initio total energy calculations for metals and semiconductors using a plane-wave basis set. *Comp. Mater. Sci.* **1996**, *6*, 15-50.
25. Kresse, G.; Hafner, J., Abinitio Hellmann-Feynman molecular-dynamics for liquid-metals. *J. Non-Cryst. Solids* **1993**, *156*, 956-960.
26. Perdew, J. P.; Burke, K.; Ernzerhof, M., Generalized gradient approximation made simple. *Phys. Rev. Lett.* **1996**, *77*, 3865.
27. Blochl, P. E., Projector augmented-wave method. *Phys. Rev. B* **1994**, *50*, 17953-17979.
28. Kresse, G.; Joubert, D., From ultrasoft pseudopotentials to the projector augmented-wave method. *Phys. Rev. B* **1999**, *59*, 1758-1775.
29. Methfessel, M.; Paxton, A. T., High-Precision Sampling for Brillouin-Zone Integration in Metals. *Phys. Rev. B* **1989**, *40*, 3616-3621.
30. Becke, A. D.; Johnson, E. R., Exchange-hole dipole moment and the ospersion interaction. *J. Chem. Phys.* **2005**, *122*.
31. Steinmann, S. N.; Corminboeuf, C., A generalized-gradient approximation exchange hole model for dispersion coefficients. *J. Chem. Phys.* **2011**, *134*.
32. Steinmann, S. N.; Corminboeuf, C., Comprehensive Bench marking of a Density-Dependent Dispersion Correction. *J. Chem. Theory Comput.* **2011**, *7*, 3567-3577.
33. Momma, K.; Izumi, F., VESTA 3 for three-dimensional visualization of crystal, volumetric and morphology data. *J. Appl. Crystallogr.* **2011**, *44*, 1272-1276.
34. Kresse, G.; Gil, A.; Sautet, P., Significance of single-electron energies for the description of CO on Pt(111). *Phys. Rev. B* **2003**, *68*.
35. Feibelman, P. J.; Hammer, B.; Norskov, J. K.; Wagner, F.; Scheffler, M.; Stumpf, R.; Watwe, R.; Dumesic, J., The CO/Pt(111) puzzle. *J. Phys. Chem. B* **2001**, *105*, 4018-4025.
36. Mason, S. E.; Grinberg, I.; Rappe, A. M., First-principles extrapolation method for accurate CO adsorption energies on metal surfaces. *Phys. Rev. B* **2004**, *69*.
37. Sumaria, V.; Nguyen, L.; Tao, F. F.; Sautet, P., Optimal Packing of CO at a High Coverage on Pt(100) and Pt(111) Surfaces. *ACS Catal* **2020**, *10*, 9533-9544.
38. Talbi, D.; Chandler, G. S., Extensive ab initio study of the C_2O_2, C_2S_2, and C_2OS systems: Stabilities and singlet-triplet energy gaps. *J. Phys. Chem. A* **2000**, *104*, 5872-5881.
39. Patel, D. A.; Kress, P. L.; Cramer, L. A.; Larson, A. M.; Sykes, E. C. H., Elucidating the composition of PtAg surface alloys with atomic-scale imaging and spectroscopy. *J. Chem. Phys.* **2019**, *151*.
40. van Spronsen, M. A.; Daunmu, K.; O'Connor, C. R.; Egle, T.; Kersell, H.; Oliver-Meseguer, J.; Salmeron, M. B.; Madix, R. J.; Sautet, P.; Friend, C. M., Dynamics of Surface Alloys: Rearrangement of Pd/Ag(111) Induced by CO and O_2. *J. Phys. Chem. C* **2019**, *123*, 8312-8323.
41. Tyson, W. R.; Miller, W. A., Surface Free-Energies of Solid Metals - Estimation from Liquid Surface-Tension Measurements. *Surf. Sci.* **1977**, *62*, 267-276.
42. Chesters, M. A.; Parker, S. F.; Raval, R., Fourier-Transform Reflection Absorption Infrared-Spectroscopy of Adsorbates on Cu(100) and Cu(111). *Surf. Sci.* **1986**, *165*, 179-190.
43. Raval, R.; Parker, S. F.; Pemble, M. E.; Hollins, P.; Pritchard, J.; Chesters, M. A., FT-RAIRS, EELS and LEED Studies of the Adsorption of Carbon Monoxide on Cu(111). *Surf. Sci.* **1988**, *203*, 353-377.
44. Kuhn, W. K.; Campbell, R. A.; Goodman, D. W., Structural, Chemical, and Electronic Properties of Cu/Ta(110). *J. Phys. Chem.* **1993**, *97*, 446-453.
45. Roiaz, M.; Falivene, L.; Rameshan, C.; Cavallo, L.; Kozlov, S. M.; Rupprechter, G., Roughening of Copper (100) at Elevated CO Pressure: Cu Adatom and Cluster Formation Enable CO Dissociation. *J. Phys. Chem. C* **2019**, *123*, 8112-8121.
46. Mudiyanselage, K.; Xu, F.; Hoffmann, F. M.; Hrbek, J.; Waluyo, I.; Boscoboinik, J. A.; Stacchiola, D. J., Adsorbate-driven morphological changes on Cu(111) nano-pits. *Phys. Chem. Chem. Phys.* **2015**, *17*, 3032-3038.
47. Eren, B.; Liu, Z. Y.; Stacchiola, D.; Somorjai, G. A.; Salmeron, M., Structural Changes of Cu(110) and Cu(110)-(2 x 1)-O Surfaces under Carbon Monoxide in the Torr Pressure Range Studied with Scanning Tunneling Microscopy and Infrared Reflection Absorption Spectroscopy. *J. Phys. Chem. C* **2016**, *120*, 8227-8231.
48. Papanikolaou, K. G.; Darby, M. T.; Stamatakis, M., CO-Induced Aggregation and Segregation of Highly Dilute Alloys: A Density Functional Theory Study. *J. Phys. Chem. C* **2019**, *123*, 9128-9138.

49. Mccue, A. J.; Anderson, J. A., CO induced surface segregation as a means of improving surface composition and enhancing performance of CuPd bimetallic catalysts. *J. Catal.* **2015**, *329*, 538-546.
50. Stakheev, A. Y.; Smirnova, N. S.; Markov, P. V.; Baeva, G. N.; Bragina, G. O.; Rassolov, A. V.; Mashkovsky, I. S., Adsorption-Induced Segregation as a Method for the Target-Oriented Modification of the Surface of a Bimetallic Pd-Ag Catalyst. *Kinet. Catal.* **2018**, *59*, 610-617.
51. Vollmer, S.; Witte, G.; Woll, C., Determination of site specific adsorption energies of CO on copper. *Catal. Lett.* **2001**, *77*, 97-101.
52. Hollins, P.; Pritchard, J., Interactions of CO Molecules Adsorbed on Cu(111). *Surf. Sci.* **1979**, *89*, 486-495.
53. Hoffmann, F. M., Infrared reflection-absorption spectroscopy of adsorbed molecules *Surf. Sci. Rep.* **1983**, *3*, 107-192.
54. Kuznetsov, M. V.; Frickel, D. P.; Shalaeva, E. V.; Medvedeva, N. I., Adsorption of carbon monoxide on Ti(0001). *J. Electron. Spectrosc. Relat. Phenom.* **1998**, *96*, 29-36.
55. Hammer, B.; Norskov, J. K., Theoretical surface science and catalysis - Calculations and concepts. *Advances in Catalysis, Vol 45* **2000**, *45*, 71-129.
56. Schimka, L.; Harl, J.; Stroppa, A.; Gruneis, A.; Marsman, M.; Mittendorfer, F.; Kresse, G., Accurate surface and adsorption energies from many-body perturbation theory. *Nat. Mater.* **2010**, *9*, 741-744.
57. Patel, D. A.; Hannagan, R. T.; Kress, P. L.; Schilling, A. C.; Cinar, V.; Sykes, E. C. H., Atomic-Scale Surface Structure and CO Tolerance of NiCu Single-Atom Alloys. *J. Phys. Chem. C* **2019**, *123*, 28142-28147.
58. Darby, M. T.; Sykes, E. C. H.; Michaelides, A.; Stamatakis, M., Carbon Monoxide Poisoning Resistance and Structural Stability of Single Atom Alloys. *Top. Catal.* **2018**, *61*, 428-438.